JOURNAL OF SOLID STATE CHEMISTRY 110, 321–329 (1994)

Antiferromagnetic Ordering and Structural Characterization of the Brown Colored R_2BaCoO_5 Oxides (R = Rare Earth)

J. Hernández-Velasco, A. Salinas-Sánchez, and R. Sáez-Puche[1]

Departamento de Química Inorgánica, Facultad de Ciencias Químicas, Universidad Complutense de Madrid, 28040 Madrid, Spain

Received May 19, 1993; in revised form August 11, 1993; accepted August 12, 1993

New R_2BaCoO_5 oxides (R = rare earth) have been prepared in Ar flow, and the X-ray diffraction data reveal that they crystallize in the Nd_2BaNiO_5 structural type (space group *Immm*). The existence of dimorphism has been shown for R = Dy, Ho, Er, and Tm. A comparative study of the influence of the rare earth size on the structural parameters is presented for this family of compounds. The relative stability of these oxides is discussed from the variation of the so-called global instability index (GII) calculated using the bond valence method. The GII values around 0.2 v.u. are indicative of the high stress present in this structure. The magnetic properties of these oxides have been studied from magnetic susceptibility measurements and one-dimensional antiferromagnetic correlations in the Co^{+2} sublattice are presented around the room temperature, while three-dimensional antiferromagnetic interactions in both R^{+3} and Co^{+2} sublattices have been observed at lower temperatures ($T_{Néel}$ < 40 K) in this family of oxides. This behavior is explained considering the crystal structure of these compounds and the electronic states of the Co^{+2} and R^{+3} cations.

INTRODUCTION

Two different structural types have been described for the R_2BaCoO_5 oxides, depending on the rare earth cation R^{+3} size (1–3).

The green colored R_2BaCoO_5 oxides (R = Dy, Ho, Er, Tm, Yb, Lu, and Y) crystallize into the Sm_2BaCuO_5 structural type, with orthorhombic symmetry, space group *Pnma*, Z = 4, with the cobalt located in isolated distorted (CoO_5) square pyramids (1, 3, 4). These compounds are isostructural with the well-known R_2BaCuO_5 oxides (5–8).

On the other hand, the brown colored R_2BaCoO_5 phases (R = Nd, Sm, Gd, Dy, and Er) crystallize into the Nd_2BaNiO_5 structure type, with orthorhombic symmetry, space group *Immm*, Z = 2, showing as its main structural feature the existence of one-dimensional arrangement of vertex-sharing (CoO_6) flattened octahedra running parallel to the crystallographic a-axis of the structure; these octahedra chains are interlocked with monocapped trigonal prisms of (RO_7), while the barium cations are surrounded by ten oxygen atoms forming bicapped square prisms (BaO_{10}), as shown in Fig. 1.

Moreover, the existence of dimorphism has been reported recently for the R_2BaCoO_5 oxides with R = Dy, Ho, Er, and Tm (4, 9–11), analogous to the case of the R_2BaNiO_5 family when R = Tm, Yb, and Lu (12–15), in which both structures can be presented by these oxides, and it depends on the different synthesis conditions.

The distortion away from the ideal octahedral coordination about Co in the case of the *Immm* oxides gives rise to unusually short Co–O–Co distances along the a-axis, around 3.75 Å (4, 10), and for this reason interesting magnetic properties are expected for these R_2BaCoO_5 oxides, bearing in mind the magnetic behavior that we have reported earlier for the isostructural R_2BaNiO_5 oxides. In this sense, the Y_2BaNiO_5 has been considered to be a one-dimensional (1D) antiferromagnet, and interchain interactions have not been detected down to 1.5 K. However, when the diamagnetic Y^{+3} is substituted by a paramagnetic rare earth cation (Nd–Tm) both sublattices, R^{3+} and Ni^{2+}, become three-dimensional (3D) antiferromagnetic ordered at temperatures about 40 K (16–21).

The main purposes of this paper are the study of the magnetic properties of these *Immm* oxides and the analysis of their structural characteristics; the former aspect has been performed from magnetic susceptibility measurements, and the latter by means of X-ray diffraction data. The relative stability of the different R_2BaCoO_5 oxides has been also analyzed, using the bond valence method proposed by Brown and Alttermatt (22, 23).

EXPERIMENTAL

Immm R_2BaCoO_5 oxides were obtained by solid state reaction from a stoichiometric mixture of R_2O_3 (99.99%), $CoCO_3 \cdot nH_2O$ (99.999%), and $BaCO_3$ (A. R. Grade). The samples were ground and heated under argon flow due to the instability of Co^{+2} in air at high temperatures; the time

[1] To whom correspondence should be addressed.

0022-4596/94 $6.00

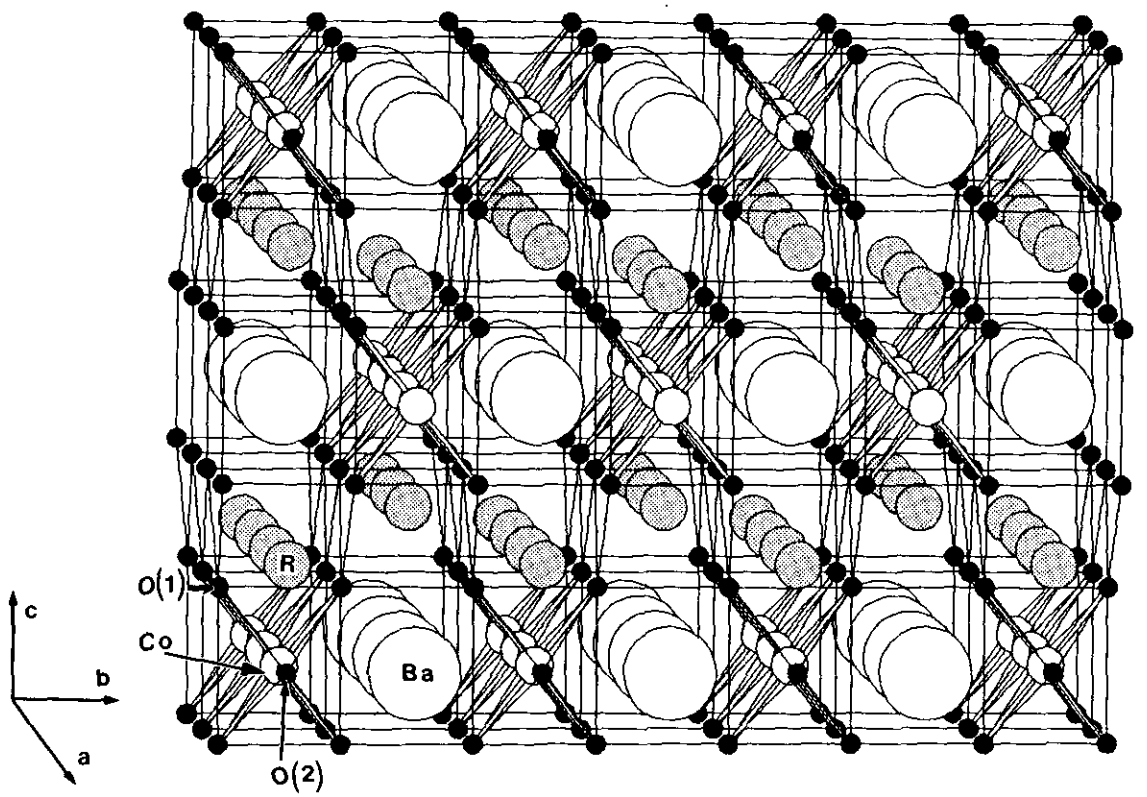

FIG. 1. Crystal structure of the *Immm* R_2BaCoO_5 oxides along the *a*-axis showing the chains of corner-sharing (CoO_6) flattened octahedra.

and temperature of firing for R = Nd–Gd were 12 hr and 1000°C. The samples were then reground to enhance the homogeneity, and a second thermal treatment for 12 hr at 1200°C and finally a third for 12 hr at 1350°C were carried out. In the case of the *Immm* R_2BaCoO_5 oxides, where R = Dy–Tm, the synthesis was done at 910°C for 12 hr, and it is worth noting that they are very critical conditions, because either higher temperatures or longer times of heating yield to the green *Pnma* R_2BaCoO_5 oxides (4, 10).

X-ray powder diffraction patterns were obtained using a Siemens Kristalloflex K810 diffractometer and a D-500 goniometer provided with a secondary graphite monochromator and CuK_α radiation. The data were collected by step scanning over an angular range of $10° < 2\theta < 120°$, in increments of 0.04° and a counting time of 15 sec per step. All the data were analyzed with the Rietveld method using the program "FULLPROF" (24). The profile function used for describing the peak shape was a pseudo-Voigt type and no preferred orientations were taken into account.

The magnetic susceptibility measurements were performed in the 4.2–300 K temperature range, with a fully automatic DSM8 magneto-susceptometer based on the Faraday method. The setup was calibrated with $Hg[Co(SCN)_4]$, $Gd_2(SO_4)_3 \cdot 8H_2O$, and $NH_4Cr(SO_4)_2 \cdot 12H_2O$ as standards. The maximum magnetic field was 14 kG with $HdH/dz \approx 24\ kG^2 \cdot cm^{-1}$. The data were corrected for ionic diamagnetism taking the values in $emu \cdot mole^{-1}$ of -18×10^{-6} for R^{+3}, -32×10^{-6} for Ba^{+2}, -16×10^{-6} for O^{-2}, and -12×10^{-6} for Co^{+2} (25).

RESULTS AND DISCUSSION

1. Structural Characterization

X-ray powder diffraction data obtained for the *Immm* R_2BaCoO_5 (R = Nd, Sm, Eu, Gd, Dy, Ho, Er, Tm) oxides reveal that they are single phases excepting the cases of the Er and the new Ho and Tm compounds, which present small amounts of the high-temperature *Pnma* R_2BaCoO_5 phases. Work is now in progress in order to find the appropriate synthesis conditions to obtain these low-temperature phases as pure compounds.

As an example, in Fig. 2, the pattern of the novel Eu_2BaCoO_5 oxide is shown; all the reflections were indexed on the *Immm* space group, and the main interatomic distances and atomic positions are given in Table 1.

The lattice parameters obtained for these oxides are given in Table 2, and fully agree with those previously reported by Müller-Buschbaum *et al.* (1–3). As was expected, assuming the ionic model, the unit cell dimensions *a*, *b*, and *c*, and the lattice volume *V*, decrease linearly as a function of the rare earth ionic radius (26) in going

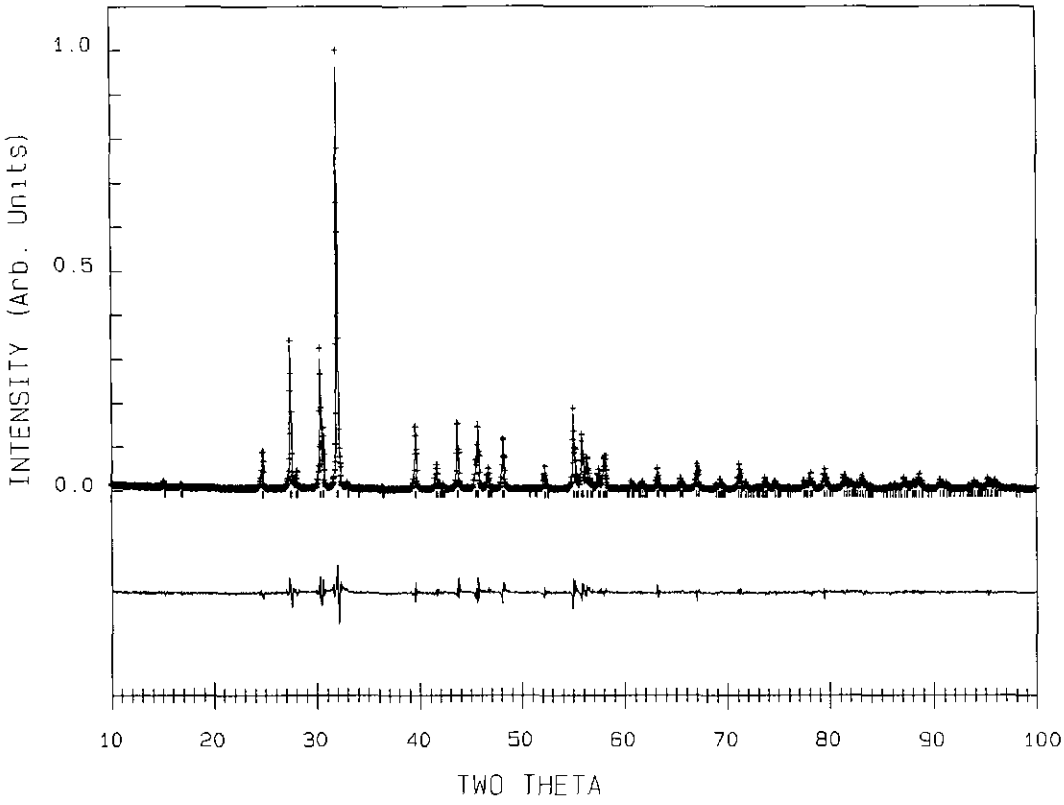

FIG. 2. X-ray powder diffraction pattern of the new Eu_2BaCoO_5 oxide. Points represent the experimental data and the solid line is the calculated profile. A difference curve is plotted at the bottom. Vertical marks represent the position of allowed Bragg reflections.

from Nd^{+3} to Er^{+3}, which is concordant with the lanthanide contraction (Fig. 3). This variation is less marked in the a parameter, about ≈ 0.07 Å from Nd to Er, than in the case of the others, i.e., $\Delta b \simeq 0.19$ Å and $\Delta c \simeq 0.38$ Å; furthermore, it is worth mentioning the fact that the b/c ratio stays essentially constant, compared to the a/c ratio which changes by over 1%. This effect can be explained by considering the structure of these compounds; in this way the smaller variation observed in the a parameter can be justified taking into account that the (CoO_6) flattened octahedra are placed along this direction. These distorted polyhedra share the O(2) axial, which is bounded to both lanthanide and barium cations, being the apex of the monocapped trigonal prisms (RO_7) and bicapped tetragonal prisms (BaO_{10}), as can be observed in Fig. 1.

The very short Co–O(2) distances (Table 3) compared with the R–O(2) distances, about 2.40 Å, justify that the substitution from Er^{+3} to Nd^{+3}, in going to larger R^{+3},

TABLE 1

Bond Lengths M–O (Å) and Atomic Positions in the Asymmetric Unit of the New *Immm* Eu_2BaCoO_5 Oxide Obtained from X-Ray Powder Diffraction Data

Atom	Site	x	y	z
Ba	2*a*	0.0	0.0	0.0
Eu	4*j*	0.5	0.0	0.704(1)
Co	2*c*	0.5	0.5	0.0
O(1)	8*l*	0.0	0.753(2)	0.356(1)
O(2)	2*d*	0.5	0.0	0.5
Eu–O(1)	2.313(11)	(×2)		
Eu–O(1)	2.451(7)	(×4)	R_p	16.4
Eu–O(2)	2.372(1)	(×1)	R_{wp}	18.9
Ba–O(1)	2.972(9)	(×8)	R_{exp}	12.42
Ba–O(2)	2.9391(1)	(×2)	χ^2	2.32
Co–O(1)	2.237(11)	(×4)	R_b	5.29
Co–O(2)	1.8881(1)	(×2)	Q	0.26(3)

Note. Reliability factors (%) and overall isotropic temperature factor Q (Å^2) are also included.

TABLE 2

Lattice Parameters Obtained for the *Immm* R_2BaCoO_5 Oxides

Compound	a (Å)	b (Å)	c (Å)
Nd_2BaCoO_5	3.8058(1)	5.9577(2)	11.8022(3)
Sm_2BaCoO_5	3.7855(1)	5.9017(2)	11.6989(3)
Eu_2BaCoO_5	3.7761(1)	5.8782(2)	11.6515(3)
Gd_2BaCoO_5	3.7650(1)	5.8571(2)	11.6301(3)
Dy_2BaCoO_5	3.7475(3)	5.8039(4)	11.5082(7)
Ho_2BaCoO_5	3.7362(3)	5.7800(4)	11.4729(7)
Er_2BaCoO_5 (Ref. 3)	3.734(1)	5.770(2)	11.421(4)

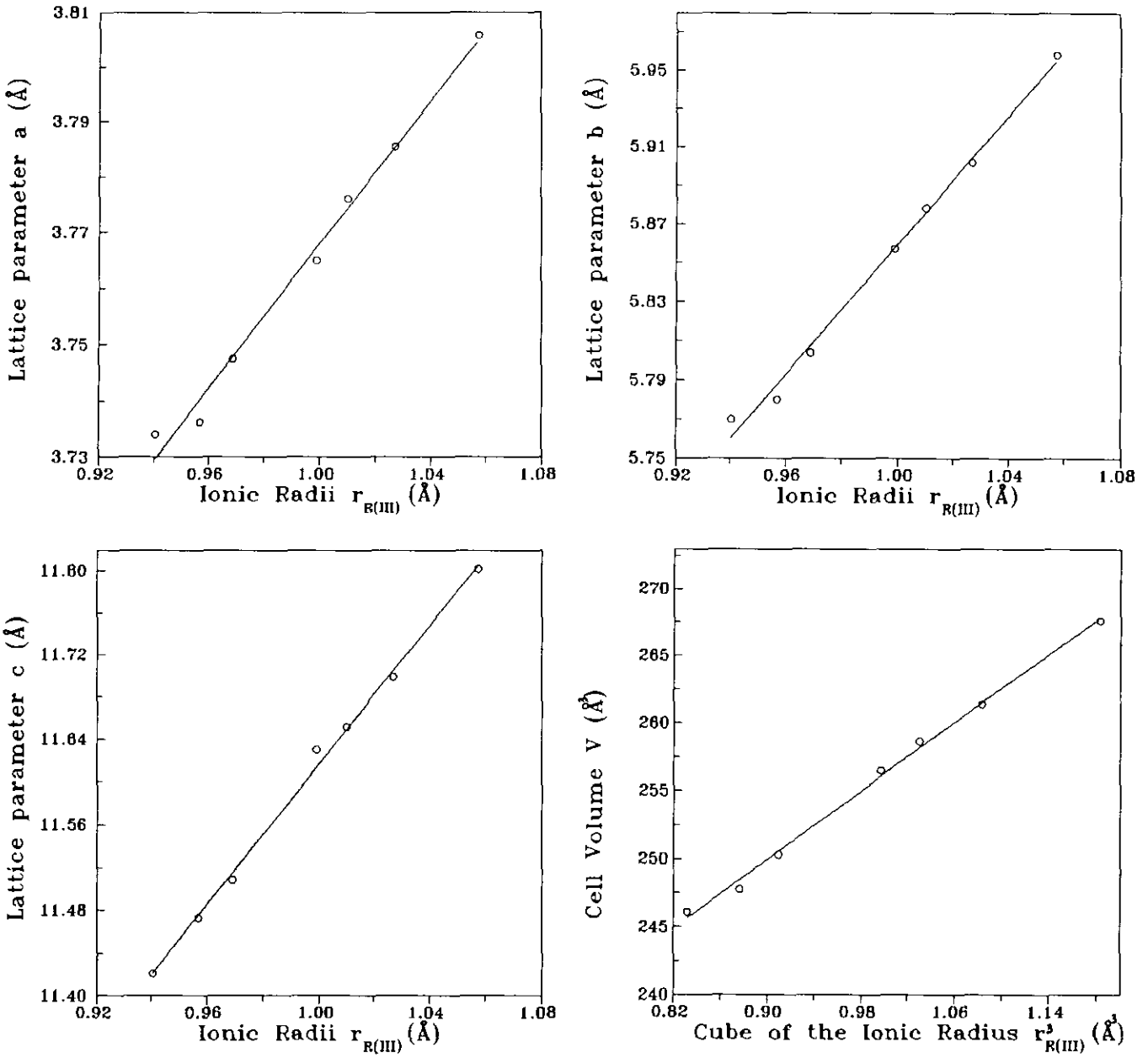

FIG. 3. Variation of lattice parameters and volume of the unit cell versus rare earth ionic radius.

TABLE 3
Bond Lengths Co–O in the Octahedra [CoO_6] of the *Immm* R_2BaCoO_5 Oxides

Distance (Å)	Nd_2BaCoO_5	Sm_2BaCoO_5	$Eu_2BaCoO_5^a$	Gd_2BaCoO_5	Dy_2BaCoO_5	Er_2BaCoO_5
Co–O(1) equatorial	2.253(10)	2.244(10)	2.237(11)	2.238(22)	2.215(16)	2.221(25)
Co–O(2) axial	1.904(1)	1.894(1)	1.8881(1)	1.885(1)	1.877(1)	1.867(1)
$\frac{[Co–O(2)]}{[Co–O(1)]}$	0.845	0.844	0.844	0.842	0.847	0.841

Note. Also included is the ratio Co–O axial/equatorial distances.

[a] Obtained by means of X-ray powder diffraction data; the remaining distances are the previously reported from single crystal X-ray diffraction results (1–3).

will not affect the Co–O(2) bond very much, and the Co–O(2)–Co distance, which is the a parameter, will only change in small amounts.

By contrast, the variation of the lattice constants b and c is due to the fact that the (RO_7) polyhedra share two edges of the quadrangular face along the b-axis, forming rows with the cap alternating along the c-axis; these rows are connected by the oxygen of the cap, namely O(2), giving rise to the tetragonal prisms in which the Ba^{+2} are located. Along the b-axis two (RO_7) polyhedra are involved, while along the c-axis there are four (RO_7) prisms forming the unit cell. This explains the larger variation observed in c, which is double that of the b variation and this is approximately triple that of the a variation.

On the other hand, the analysis of the Co–O distances obtained from single crystal X-ray diffraction data, (1–3) Table 3, shows that the Co–O(1) equatorial bond length variation is very small; however, it is accompanied by the change in the basal angle O(1)–Co–O(1), which is always smaller (about 80°) than the expected right angle of a regular octahedron, whose ideal O_h symmetry is diminished to D_{4h} because the axial Co–O(2) distances are much shorter than the equatorial ones. The angular distortion, which is mainly due to the rare earth atoms, gives rise finally to a D_{2h} point symmetry for the (CoO_6) units.

A description of these distortions has been given for the isostructural R_2BaNiO_5 compounds by Burdett and Mitchell (27) who by means of semi-empirical quantum chemistry calculations justify the preference for two short distances, Ni–O(2) axial, and four longer, Ni–O(1) equatorial, for these Ni oxides. However, from the energy calculations reported there, it is inferred that an arrangement of vertex-sharing octahedral chains in which the metal electronic configuration is d^7, as in the case of the Co^{+2}, reverses that preference, favoring two long and four shorter M–O distances. This prediction fully disagrees with the experimental results; even the cobalt octahedra (CoO_6) are more flattened than the nickel ones (NiO_6), as can be observed in Table 3, if we compare the ratio between the axial and equatorial distances, which remains approximately constant in these families of compounds and takes the $\Delta\{d[M\text{–O(2)}]/d[M\text{–O(1)}]\} \simeq 0.86$ average value for the Ni oxides (15) while it is lower, about $\Delta \simeq 0.844$ for the Co octahedra, indicating that the latter are more distorted.

In order to complete the study of the structural characteristics of the *Immm* R_2BaCoO_5 oxides, we have applied the bond valence method (22, 23). The calculations have been made using the earlier reported interatomic distances obtained from single crystal X-ray diffraction data (1–3) because of their better accuracy in the location of oxygen atoms compared with the results from X-ray powder diffraction data and due to the impossibility of using neutron diffraction techniques since the absorption cross-sections are too high in the case of the Sm, Eu, Gd, and Dy elements.

The phenomenological relation between the bond length (R_{ij}) and the formal valence of a bond is $S_{ij} = \exp[(R_o - R_{ij})/B]$, where R_o is a parameter characteristic of the particular anion–cation pair, which is known (28), and $B = 0.37$ is a "universal" constant for all kinds of atoms. The bond valence sum rule (VSR) establishes that the formal valence (charge) of the i-cation (V_i) must be equal to the sum of bond valences around the cation, which can be expressed as $V_i = \sum_j S_{ij}$. The method is very useful because the VSR is satisfied by many inorganic compounds. The verification of the rule takes place if the stress introduced by the coexistence of different structural units can be released by the existence of enough degrees of freedom in the crystallographic structure. The rule is violated in the case of highly symmetric structures with several atoms in special positions, or containing ions with strong Jahn–Teller effect, or in compounds presenting disorder or vacancies. From the deviations of the valence sum around each ion with respect to the expected value (the formal valence), there is a measurement of possible instabilities, stress in the bonds or unusual features in the crystal structure.

Table 4 shows the bond valence sums for the different *Immm* R_2BaCoO_5 oxides; it can be observed that the valence sums around barium increase with the decrease of the ionic size of the rare earth cation. The same behavior is observed for the values around the cobalt, while for the lanthanide cations a decrease is observed when the atomic number of the rare earth increases.

TABLE 4
Bond Valence Sums (esd < 0.01 v.u.) and Global Instability Indices (GII) Obtained for Some *Immm* R_2BaCoO_5 Oxides (in Valence Units)

Atom	Nd_2BaCoO_5	Sm_2BaCoO_5	Eu_2BaCoO_5	Gd_2BaCoO_5	Dy_2BaCoO_5	Er_2BaCoO_5
Ba	1.531	1.577	1.614	1.628	1.725	1.727
Co	2.006	2.058	2.094	2.102	2.186	2.204
R	3.018	2.993	2.952	2.979	2.909	2.926
GII	0.271	0.247	0.231	0.223	0.199	0.201

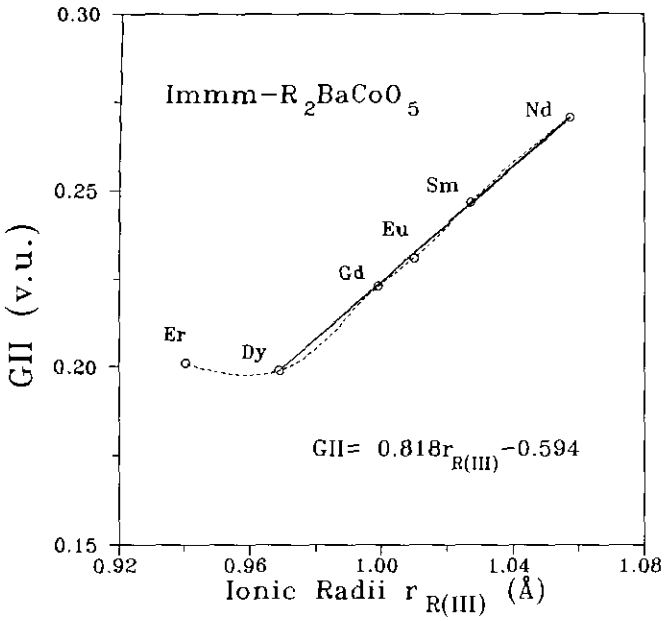

FIG. 4. Global instability index (GII) in valence units versus ionic radii of the trivalent rare earth cations. The dashed line is the fitting of all the experimental points with a cubic spline. The solid line represents a linear function from least-squares fitting the data from Dy to Nd.

The root mean square of the bond valence sum deviations for all the atoms present in the asymmetric unit is a measure of the extent to which the VSR is violated over the whole structure (29). This value is called "global instability index" (GII):

$$\mathrm{GII} = \left\{ \sum_{i=1}^{n} [(\Sigma_j S_{ij} - V_i)^2]/N \right\}^{1/2}.$$

The obtained values are given in Table 4, and we have plotted the variation of GII vs the rare earth R^{+3} ionic radius (26) in Fig. 4. It can be observed that when the ionic radius of the lanthanide cation increases from Dy to Nd, the instability index goes up taking its maximum value (lower stability) for the Nd_2BaCoO_5 oxide, and a linear behavior is clearly shown. This could explain that for R with larger ionic radius than Nd, this structure type seems not to exist; for example the GII of a hypothetical *Immm* La_2BaCoO_5 compound will take the value of 0.306 v.u. ($r_{La(III)}$ = 1.10 Å (26)) obtained from least-squares fitting the linear range of GII vs R^{+3} ionic radii, and this high amount justifies the nonexistence of this compound. As suggested by Brown (29) and Armbruster *et al.* (30), GII values higher than 0.2 v.u. indicate the presence of intrinsic strains large enough to cause instability at room temperature, and for this reason we conclude that these oxides are under very high internal stress and may be metastable.

Nevertheless, when the ionic radius of the rare earth is smaller than that of Dy, the GII appears to remain constant; although there are few data, similar behavior has been observed in the Ni oxides (15). However, for these lanthanide cations (R = Dy, Ho, Er, Tm), in which both *Pnma* and *Immm* forms have been observed, the Sm_2BaCuO_5 type seems to be more stable; for example, the GII value obtained for the *Pnma* Ho_2BaCoO_5 oxide is $\simeq$ 0.0703 v.u. and for the other cobalt oxides that crystallize with this structural type, the GII takes values around 0.1 v.u. indicating this higher stability (31). Analogous behavior has been observed for the *Pnma* R_2BaCuO_5 compounds (32) with lower values of the GII than in the case of those obtained for the *Immm* R_2 $BaNiO_5$ oxides (15).

2. *Magnetic Properties*

The magnetic moments obtained for some *Immm* R_2Ba CoO_5 are listed in Table 5, and they are in good agreement with those expected for the rare earth R^{+3} only contribution; the small differences are due to the cobalt contribution which is much smaller than that expected from Co^{+2} with $S = \frac{3}{2}$, which can be explained by 1D-antiferromagnetic order around the room temperature analogous to that observed in the isostructural R_2BaNiO_5 oxides (16–21). These interactions of antiferromagnetic character are greatly favorable if we consider the structure of these R_2BaCoO_5 oxides, in which, as can be observed in Table 3, the surprisingly short Co–O(2)–Co distances in straight angle are responsible for the strong superexchange due to the supported overlapping at 180° between the oxygen p-orbitals and the cobalt e_g orbitals, which according to Goodenough's rules (33) will enhance the antiferromagnetic interactions.

This low-dimensional antiferromagnetic behavior at high temperature is a common characteristic of all the *Immm* R_2BaCoO_5 oxides studied. However, at lower temperatures, the situation is more complex and depends on

TABLE 5

Experimental (μ_e) and Calculated (μ_c) Magnetic Moments, Weiss Constants (θ), and Temperatures at Which the Susceptibility is Maximum ($T\chi_{max}$) for *Immm* R_2BaCoO_5 Oxides

Compound	μ_e (BM)	μ_c (BM)	θ (K)	$T\chi_{max}$ (K)
Nd_2BaCoO_5	3.80	3.62	−25.0	15.2
Sm_2BaCoO_5	2.84[a]	1.6[b]	—	39.8, 238.3
Eu_2BaCoO_5	3.70[a]	3.5[b]	—	—
Gd_2BaCoO_5	8.26	7.94	−3.5	—
Dy_2BaCoO_5	10.66	10.65	−5.3	10.4

[a] Observed at room temperature.

[b] Calculated from Van Vleck and Frank's equation; the remaining theoretical moments have been obtained by the relation $\mu_c = g\sqrt{J(J+1)}$.

the particular lanthanide cation presented in the R_2BaCoO_5 oxide.

In the case of the Nd and Dy compounds the variation of the magnetic susceptibility with the temperature is shown in Figs. 5 and 6; the existence of net maxima can be observed at 15.2 and 10.4 K, respectively, and above these temperatures the susceptibility follows a Curie–Weiss law. The presence of these maxima and the negative values obtained for the Weiss constants are indicatives of 3D-antiferromagnetic ordering in which both rare earth and cobalt sublattices appear to be involved, and the pathway through which these interactions take place is probably superexchange of the type Co^{2+}–O–R^{3+}–O–Co^{2+}.

The 3D antiferromagnetic character of these interactions has been confirmed from preliminary neutron diffraction data in the case of the Nd_2BaCoO_5 oxide (31, 34). More work is now in progress in order to establish the Néel temperature and the magnetic structure of this oxide.

In the case of the Gd_2BaCoO_5 oxide, although the magnetic susceptibility vs T plot does not show the presence of a maximum, the existence of antiferromagnetic interactions can be inferred from the observed deviations upward from linearity in the χ^{-1} vs T plot below 40 K (Fig. 7); since, in the $^8S_{7/2}$ ground term of the Gd^{+3} free ion under the crystal field influence, the splitting of energy levels should be very small and its effect can be neglected, in the absence of any magnetic cooperative interactions the magnetic moment must be independent of the temperature and given by Hund's equation (35). Moreover, there are other points which agree with the proposed 3D-antiferromagnetic ordering, which are on the one hand the rather small $\chi * T$ value obtained at 4.2 K, about $\simeq$ 2 emu·mole^{-1}·K, and on the other hand the negative value of the Weiss constant, $\simeq -3.5$ K.

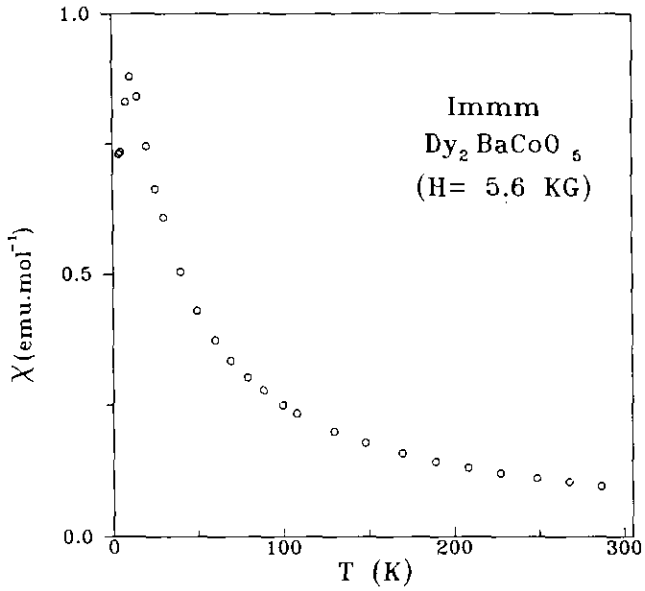

FIG. 6. Temperature dependence of the molar magnetic susceptibility for the Dy_2BaCoO_5 oxide.

The most different magnetic behavior exhibited by these *Immm* oxides is that corresponding to the Eu_2BaCoO_5 case. Figure 8 shows the molar magnetic susceptibility variation with the temperature for this compound and it can be explained by considering that the Eu^{+3} ion has a nonmagnetic $^7F_0$ ground state. The spacing between the different multiplet levels is not too large compared with the thermal energy kT and therefore not all the ions are

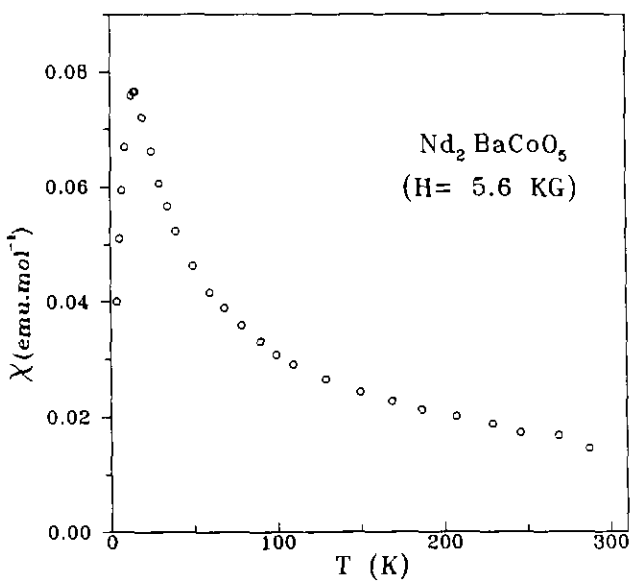

FIG. 5. Temperature dependence of the molar magnetic susceptibility for the Nd_2BaCoO_5 oxide.

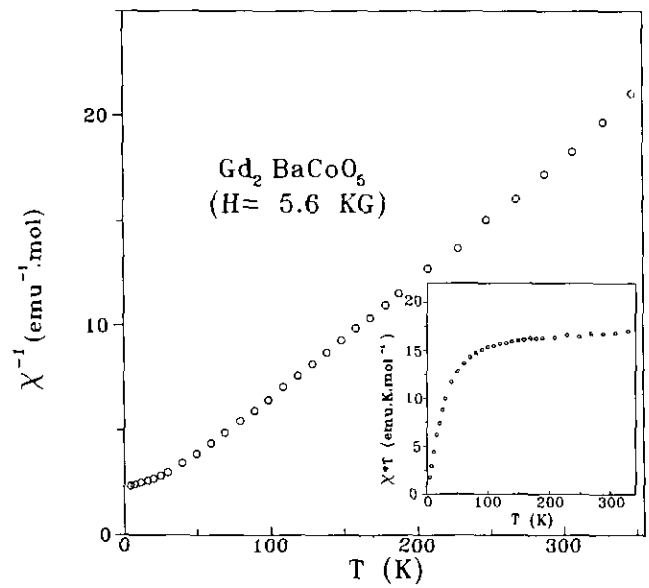

FIG. 7. Temperature dependence of the reciprocal molar magnetic susceptibility for the Gd_2BaCoO_5 oxide. The inset shows the $\chi \cdot T$ vs T plot.

in their ground state; the excited states with larger J values also contribute to the magnetic susceptibility, and the magnetic moment will be a function of the temperature (35–37). The variation of the magnetic susceptibility shown in Fig. 8 follows the characteristic behavior of the Eu^{+3} free ion, and the plateau observed in the susceptibility below 100 K is due to the second-order temperature-independent term of the Van Vleck formula (38) arising from the population of the nonmagnetic $^7F_0$ ground term. The Co^{+2} does not contribute to the susceptibility indicating the 1D antiferromagnetic order along the crystallographic a-axis as mentioned earlier. Nevertheless, there is no evidence of 3D antiferromagnetic ordering at low temperatures, which can be explained taking into account that the superexchange interactions through the pathways Co^{+2}–O–R^{+3}–O–Co^{+2} are not promoted by the nonmagnetic Eu^{3+} ($^7F_0$) ion, as was expected.

Figure 9 shows the temperature dependence of the magnetic susceptibility for the Sm_2BaCoO_5 oxide, and the presence of two maxima at $\simeq$ 240 and $\simeq$ 40 K is observed. Although this behavior appears to be uncommon, when it is compared with the remaining *Immm* R_2BaCoO_5 oxides discussed above, however, it can be explained in the same way. The broad maximum centered around 240 K can be attributed to the 1D antiferromagnetic correlations in the (CoO_6) chains. These interactions which are also operative in the other *Immm* R_2BaCoO_5 oxides are masked by the strong paramagnetic signals coming from the R^{+3} cations. In this case, the magnetic moment of Sm^{+3}, which is 1.6 BM at room temperature, is even smaller than that of Co^{+2}, about 4.9 BM, and it permits the observation of the Co^{+2} contribution. In this way, Table 5 shows that the

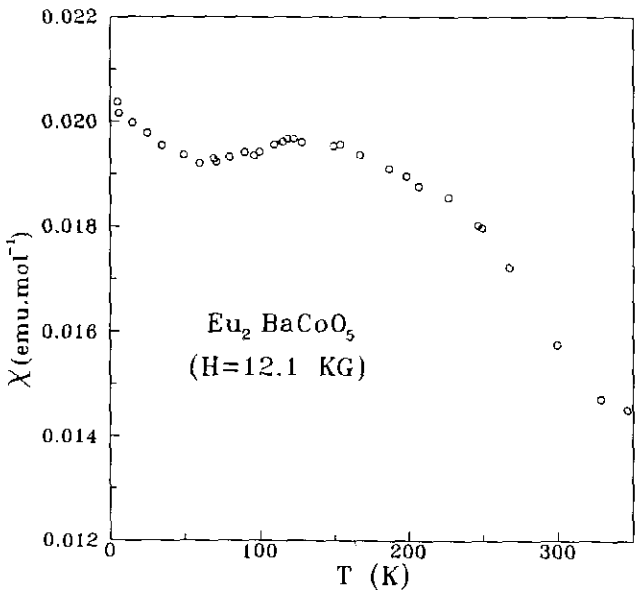

FIG. 8. Temperature dependence of the molar magnetic susceptibility for the Eu_2BaCoO_5 oxide.

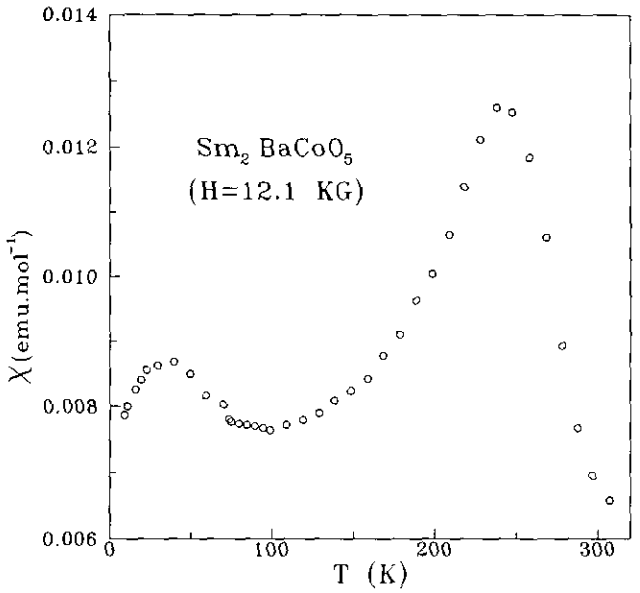

FIG. 9. Temperature dependence of the molar magnetic susceptibility for the Sm_2BaCoO_5 oxide.

experimental magnetic moment for Sm_2BaCoO_5 is larger than the calculated for Sm^{+3} only contribution, while in the case of the remaining oxides both μ_e and μ_c are almost the same.

It is worth mentioning that in the *Pnma* R_2BaCoO_5 oxides, 1D antiferromagnetic order has not been observed due to the very different crystal structure that is adopted, which avoids this type of cooperative interactions, while 3D antiferromagnetism at low temperatures is presented in some cases (34, 39).

CONCLUSIONS

In summary, fascinating structural features are shown in the R_2BaCoO_5 family of oxides and we have studied in detail how the structure varies with the presence of different rare earth elements in this system; in particular we observe a highly distorted octahedron (CoO_6) with two short axial distances and four longer basal ones, which slightly increases its volume while the axial/equatorial ratio in going to larger R^{+3} lanthanide cations remains almost constant. The variation of the global instability index of the structure has been studied and also depends on the rare earth size. The GII value linearly rises with the increase of the lanthanide ionic radius, which explains the nonexistence of the *Immm* La_2BaCoO_5 oxide. Furthermore, the higher stability of the *Pnma* R_2BaCoO_5 oxides is justified due to the higher GII values in the *Immm* oxides.

The very interesting magnetic properties exhibited by these oxides have been explained considering the structure that they present. In this way, the chains of (CoO_6)

flattened octahedra and the extremely short Co–O–Co distances justify the behavior of the Co^{+2} sublattice as one-dimensional system antiferromagnetically ordered below 300 K. On the other hand, 3D antiferromagnetic interactions have been observed in some of these oxides at lower temperatures ($T_{Néel} < 40$ K) in which both cobalt and the rare earth sublattices are involved.

ACKNOWLEDGMENT

We thank the CICYT (Project MAT92-0374) for financial support.

REFERENCES

1. H. Mevs and Hk. Müller-Buschbaum, *Z. Anorg. Allg. Chem.* **573,** 128 (1989).
2. H. Mevs and Hk. Müller-Buschbaum, *J. Less-Common Met.* **152,** 139 (1989).
3. H. Mevs and Hk. Müller-Buschbaum, *Z. Anorg. Allg. Chem.* **574,** 172 (1989).
4. R. Sáez-Puche, J. Hernández-Velasco, and F. Fernández, "Solid State Ionics, Proceedings of the 12th International Symposium on the Reactivity of Solids, Madrid, 1992," **63–65,** 922 (1993).
5. C. Michel and B. Raveau, *J. Solid State Chem.* **43,** 73 (1982).
6. S. Schiffler and Hk. Müller-Buschbaum, *Z. Anorg. Allg. Chem.* **540/541,** 243 (1986).
7. S. Schiffler and Hk. Müller-Buschbaum, *Monatsh. Chem.* **117,** 485 (1986).
8. R. Norrestam, M. Hjorth, and J. O. Bovin, *Z. Kristallogr.* **183,** 245 (1988).
9. R. Sáez-Puche, F. Fernández, and J. Hernández, *in* "2nd Italian–Portuguese–Spanish Meeting in Inorganic Chemistry." Alfamar (Portugal), March 23–27, 1992." Abstracts IS 15; R. Sáez-Puche, J. Hernández-Velasco, F. Fernández, and A. Salinas-Sánchez, *in* "4th European Conference on Solid State Chemistry. Dresden, Sept. 7–9, 1992." Abstracts C 64, p. 340.
10. J. Hernández-Velasco and R. Sáez-Puche, *J. Alloys and Compounds* **198,** 63 (1993).
11. E. Kluver and Hk. Müller-Buschbaum, *Z. Anorg. Allg. Chem.* **619,** 421 (1993).
12. A. Salinas-Sánchez, R. Sáez-Puche, J. Rodríguez-Carvajal, and J. L. Martínez., *Solid State Commun.* **78**(6), 481 (1991).
13. A. Salinas-Sánchez, R. Sáez-Puche, F. Fernández, A. Andrés, A. Lavat, and E. J. Baran, *J. Solid State Chem.* **99,** 63 (1992).
14. E. García-Matres, J. Rodríguez-Carvajal, J. L. Martínez, J. A. Alonso, A. Salinas-Sánchez, and R. Sáez-Puche, *Solid State Ionics* **63–65,** 915 (1993).
15. E. García-Matres, J. L. Martínez, J. Rodríguez-Carvajal, J. A. Alonso, A. Salinas-Sánchez, and R. Sáez-Puche, *J. Solid State Chem.* **103,** 322 (1993).
16. J. Amador, E. Gutiérrez-Puebla, M. A. Monge, I. Rasines, C. Ruíz-Valero, F. Fernández, R. Sáez-Puche, and J. A. Campá, *Phys. Rev. B* **42,** (13), 7918 (1990).
17. J. A. Alonso, J. Amador, J. L. Martínez, I. Rasines, J. Rodríguez-Carvajal, and R. Sáez-Puche, *Solid State Commun.* **76,** 467 (1990).
18. R. Sáez-Puche, J. M. Coronado, L. C. Otero-Díaz, and J. M. Martín-Llorente. *J. Solid State Chem.* **93,** 461 (1991).
19. R. Sáez-Puche, J. M. Martín-Llorente, and J. M. Coronado, *J. Less-Common Met.* **175,** 131 (1991).
20. G. G. Chepurko, Z. A. Kazei, D. A. Kudrjavtsev, R. Z. Levitin, B. V. Mill, M. N. Popova, and V. V. Snegirev, *Phys. Lett. A* **157,** 81 (1991).
21. R. Sáez-Puche, J. M. Coronado, J. M. Martín-Llorente, and I. Rasines, *Mater. Chem. Phys.* **31,** 151 (1992).
22. I. D. Brown and D. Alttermatt, *Acta Crystallogr., Sect. B* **41,** 240 (1985).
23. I. D. Brown and D. Alttermatt, *Acta Crystallogr., Sect. B* **41,** 244 (1985).
24. J. Rodríguez-Carvajal, "FULLPROF: A Program for Rietveld Refinement and Pattern Matching Analysis." Satellite Meeting on Powder Diffraction of the XV Congress of the International Union of Crystallography, Toulouse (France), 1990. Abstracts, p. 127.
25. L. N. Mulay and E. A. Boudreaux, "Theory and Applications of Molecular Paramagnetism," p. 494. Wiley, New York, 1976.
26. R. D. Shannon and C. T. Prewitt, *Acta Crystallogr., Sect. B* **25,** 925 (1969).
27. J. K. Burdett and J. F. Mitchell, *J. Am. Chem. Soc.* **112,** 6571 (1990).
28. N. E. Brese and M. O'Keeffe, *Acta Crystallogr., Sect. B* **47,** 192 (1991).
29. I. D. Brown, *Z. Kristallogr.* **199,** 255 (1992).
30. T. Armbruster, F. Röthlisberger, and F. Seifert, *Am. Mineral.* **75,** 847 (1990).
31. J. Hernández-Velasco, Master's thesis, Universidad Complutense de Madrid, Spain, 1992.
32. A. Salinas-Sánchez, J. L. García-Muñoz, J. Rodríguez-Carvajal, R. Sáez-Puche, and J. L. Martínez, *J. Solid State Chem.* **100,** 201 (1992).
33. J. B. Goodenough, "Magnetism and the Chemical Bond." Wiley, New York, 1963.
34. J. Hernández-Velasco, R. Sáez-Puche, J. Rodríguez-Carvajal, E. García-Matres, and J. L. Martínez, *J. Alloys and Compounds,* in press (1994).
35. R. L. Carlin, "Magnetochemistry." Springer-Verlag, New York, 1986.
36. J. H. Van Vleck. "Theory of Electric and Magnetic Susceptibilities." Oxford Univ. Press, Oxford, 1965.
37. A. H. Morrish, "The Physical Principles of Magnetism," R. E. Krieger, New York, 1980.
38. J. H. Van Vleck and Frank, *Phys. Rev.* **34,** 1494 (1929).
39. J. Hernández-Velasco, A. Salinas-Sánchez, F. Fernández, and R. Sáez-Puche, *J. Alloys and Compounds,* in press (1993).